Length divergence of the lattice thermal conductivity in suspended graphene nanoribbons

Arnab K. Majee and Zlatan Aksamija*

Department of Electrical and Computer Engineering, University of Massachusetts–Amherst, Amherst, Massachusetts 01003-9292, USA

(Received 21 September 2015; revised manuscript received 26 April 2016; published 14 June 2016)

Thermal properties of graphene have attracted much attention, culminating in a recent measurement of its length dependence in ribbons up to 9 μm long. In this paper, we use the improved Callaway model to solve the phonon Boltzmann transport equation while capturing both the resistive (umklapp, isotope, and edge roughness) and nonresistive (normal) contributions. We show that for lengths smaller than 100 μm, scaling the ribbon length while keeping the width constant leads to a logarithmic divergence of thermal conductivity. The length dependence is driven primarily by a ballistic-to-diffusive transition in the in-plane (LA and TA) branches, while in the hydrodynamic regime when 10 μm $< L <$ 100 μm, the contribution from the in-plane branches saturates and the out-of-plane (ZA) branch shows a clear logarithmic trend, driven by the nonresistive normal contribution. We find that thermal conductivity converges beyond $L >$ 100 μm due to the coupling between in-plane and flexural modes. This coupling leads to renormalization of ZA phonon dispersion in the long-wavelength range, preventing further divergence of thermal conductivity. We also uncover a strong dependence on sample width, which we attribute to the interplay between nonresistive normal and diffusive edge scattering in the Poisseuille flow regime. We conclude that normal processes play a crucial role in the length and width dependence of thermal transport in graphene in the hydrodynamic regime and dictate the relative in-plane (LA+TA) to out-of-plane (ZA) contribution to transport.

DOI: 10.1103/PhysRevB.93.235423

I. INTRODUCTION

In recent years, two-dimensional materials have been the subject of intense research because of their unique electronic and thermal transport behavior. Among such materials, graphene has been studied the longest and has shown the most promising properties, with the highest reported thermal conductivity (ranging from 1800 to 5300 W m^{-1} K^{-1}) [1–3] and electron mobility (intrinsic limit in the order of 10^5 cm^2/V s) [4]. Engineering graphene devices require a firm understanding of the thermal transport mechanism, which is mainly dominated by phonons [5,6] because of strong covalent sp^2 bonding, which efficiently transfers heat by lattice vibrations. Despite enormous progress in understanding the thermal transport in graphene, there are several questions yet to be answered. In three-dimensional samples, thermal conductivity converges to the bulk value of graphite when the size exceeds the mean free path (mfp) of phonons and transport becomes entirely diffusive in nature. Heat conduction in such a case is mainly governed by resistive umklapp phonon-phonon scattering rather than scattering from the rough boundaries. In contrast, a length-dependent behavior of thermal conductivity has been observed in one-dimensional (1D) and two-dimensional (2D) materials even for samples much bigger than the mean free path of phonons. There are rigorous mathematical proofs for such diverging behavior in momentum-conserving one-dimensional systems [7–10] and it has also been experimentally demonstrated for carbon nanotubes [11]. However, in 2D materials, the reason for this length divergence is still much in debate.

Recently, Xu *et al.* [12] provided experimental evidence of this length divergence for samples as long as 9 μm (around ten times greater than the average mean free path of acoustic phonons in suspended graphene) and attributed the reasons for length divergence to the reduced dimensionality and displacement of in-plane phonon populations at stationary nonequilibrium conditions. In addition, quasiballistic propagation of extremely long-wavelength acoustic phonons has been demonstrated by Mei *et al.* [13], where they have shown that about 20% of phonons have mean free path greater than 100 μm, indicating a wide ballistic to diffusive crossover regime and thermal conductivity ultimately converging to 5800 W m^{-1} K^{-1}. Nika *et al.* [14] emphasized the importance of low-frequency acoustic phonons, illustrating that with the increase in the sample size, more such low-frequency phonons can be excited, which in turn contributes to thermal conduction, thereby leading to length-dependent behavior. Lindsay *et al.* [15] explained the significance of low-frequency ZA phonons towards thermal conductivity in graphene flakes, which leads to length-dependent behavior.

In contrast to the aforementioned studies, Chen *et al.* [3] reported thermal conductivity in graphene flakes without any sample size dependence. This was attributed to large uncertainty in the measurement of thermal conductivity due to grain boundaries, wrinkles, defects, or polymeric residues in the graphene sample. Park *et al.* [16] used molecular dynamics simulations to demonstrate the length dependence over a wide range and interestingly, showing a converging behavior of thermal conductivity at 16 μm and finally reporting a macroscopic limit of heat transport in graphene flakes as 3200 W m^{-1} K^{-1}. Recently, Barbarino *et al.* [17] performed a direct atomistic simulation called approach-to-equilibrium molecular dynamics to capture thermal conductivity in large samples. They found that intrinsic thermal conductivity in monolayer graphene is upper limited. Thus, there has been both theoretical and experimental evidence of length divergence of thermal conductivity for large samples (up to a few microns), but still there has been an active debate going on about the divergence of thermal conductivity for flakes when $L \to \infty$.

*zlatana@engin.umass.edu

In this paper, we study the length and width dependence of the thermal conductivity of suspended graphene ribbons. In Sec. II we present the details of the method used to calculate thermal conductivity in graphene ribbons which is based on the full phonon dispersion and the improved Callaway model recently proposed by Allen [18]. In Sec. III we discuss our results, showing two distinct regimes of thermal transport as the length of the graphene ribbon is increased: logarithmic divergence below 100 μm, driven by the flexural branch, and convergence for lengths exceeding 100 μm caused by renormalization of the flexural branch due to coupling between in-plane and cross-plane phonons in the long-wavelength regime. We also show a strong width dependence of thermal conductivity in graphene ribbons due to the nonresistive normal contribution. Finally, in Sec. IV we conclude and comment on the connection of our work to the newly discovered hydrodynamic regime of thermal transport in two-dimensional materials.

II. THERMAL CONDUCTIVITY CALCULATED FROM IMPROVED CALLAWAY MODEL

A. Improved Callaway model

Several techniques have been employed to model thermal transport in graphene such as nonequilibrium molecular dynamics (NEMD) [19,20], non-equilibrium Green's functions (NEGF) [21,22] and Boltzmann transport equation simulations [23–25]. In our work, we have used the solution of a full phonon Boltzmann transport equation (pBTE) in order to calculate thermal conductivity in graphene nanoribbons (GNRs) based on Allen's improved Callaway model. The steady state phonon BTE can be written as

$$\vec{v}(\vec{q},b)\cdot\nabla_{\vec{r}}N_{\vec{q}} = -\frac{N_{\vec{q}}-N^0_{\vec{q}}}{\tau_C(\vec{q},b)} - \frac{N_{\vec{q}}-N^*_{\vec{q}}}{\tau_N(\vec{q},b)}, \tag{1}$$

where $N_{\vec{q}}$ is the number of phonons with wave vector $\vec{q}$, $N^0_{\vec{q}}$ is equilibrium Bose-Einstein distribution, $\vec{v}(\vec{q},b)$ is the group velocity, and $\tau_C(\vec{q},b)$ is the effective relaxation time due to all scattering mechanisms (which include phonon-phonon scattering, isotope scattering, impurity scattering, and edge roughness scattering). Anharmonic phonon-phonon interactions can be categorized into umklapp (U) and normal (N) processes. Umklapp processes (which destroy crystal momentum) relax the nonequilibrium distribution to the final zero-current equilibrium Bose-Einstein distribution and are resistive in nature, whereas N processes conserve crystal momentum and relax the perturbed distribution to a flowing equilibrium ($N^*_{\vec{q}}$). In materials like graphene, where the Debye temperature is very high (about 2100 K) [26,27], these momentum-conserving normal processes have been shown to play a significant role in the context of heat conduction [15].

The $N^*_{\vec{q}}$ term represents a flowing equilibrium to which the distribution evolves under the influence of momentum-conserving normal phonon-phonon processes. Flowing equilibrium can be envisioned as a hydrodynamic component [28]—while momentum-destroying resistive processes such as umklapp scattering tend to relax the nonequilibrium distribution back to its equilibrium Bose-Einstein form; the nonresistive normal processes conserve crystal momentum and hence cannot fully destroy the heat flux, but only redistribute it among the phonon modes. Umklapp scattering, isotope scattering, and edge roughness scattering all destroy crystal momentum; thus all these resistive processes can be grouped under $\tau_U^{-1}(\vec{q},b)$. The combined scattering rate is given as the sum of resistive and nonresistive terms $\tau_C{}^{-1}(\vec{q},b) = \tau_U{}^{-1}(\vec{q},b) + \tau_N{}^{-1}(\vec{q},b)$, where $\tau_N{}^{-1}(\vec{q},b)$ is the scattering rate due to normal scattering. The thermal conductivity expression includes an extra term over the Debye term and is called the N-drift term, which accounts for additional conductivity from the nonresistive normal processes so that $K_{\rm tot} = K_C + K_N$.

Allen [18] improved the Callaway model [29] and proposed a modified expression in order to correctly include the contribution of resistive (processes which destroy crystal momentum) and nonresistive (which conserves crystal momentum) processes towards thermal conductivity and added a correction term ($\frac{\lambda_1\lambda_2}{\lambda_3}$), summed over all the branches b, to the Debye term K_C. The accuracy of the improved Callaway model (ICM) was compared with the iterative solution of the BTE by Ma *et al.* [30], to find that the trend of lattice thermal conductivity against temperature obtained from the ICM compares more favorably to the full iterative BTE solution than the relaxation time approximation (RTA) or the original Callaway model, especially in those cases where normal scattering is significant.

The modified ICM expressions are given as

$$K_{\rm tot} = K_C + K_N = K_C + \sum_b \frac{\lambda_{1,b}\lambda_{2,b}}{\lambda_{3,b}}, \tag{2}$$

where K_C is the Debye term, arising from the RTA and sometimes also called K_{RTA}, and is given by

$$K_C = \frac{1}{A\delta}\sum_{\vec{q},b}\hbar\omega_{\vec{q},b}v_\parallel^2(\vec{q},b)\tau_C(\vec{q},b)\frac{\partial N_{\vec{q}}}{\partial T}, \tag{3}$$

where A is the area of the GNR sheet, δ (=0.335 nm) is the thickness of the graphene monolayer [31], and $v_\parallel$ is the velocity of phonons along the ribbon direction. The correction terms can be expressed as

$$\lambda_{1,b} = \frac{1}{A\delta}\sum_{\vec{q}} v_\parallel(\vec{q},b)q_\parallel\tau_C(\vec{q},b)\frac{\partial N_{\vec{q}}}{\partial T}, \tag{4}$$

$$\lambda_{2,b} = \frac{1}{A\delta}\sum_{\vec{q}} v_\parallel(\vec{q},b)q_\parallel\left[\frac{\tau_C(\vec{q},b)}{\tau_N(\vec{q},b)}\right]\frac{\partial N_{\vec{q}}}{\partial T}, \tag{5}$$

$$\lambda_{3,b} = \frac{1}{A\delta}\sum_{\vec{q}} \left(\frac{q_\parallel^2}{\hbar\omega_{\vec{q},b}}\right)\left[\frac{\tau_C(\vec{q},b)}{\tau_U(\vec{q},b)}\right]\frac{\partial N_{\vec{q}}}{\partial T}, \tag{6}$$

where $q_\parallel$ is the component of the wave vector along the ribbon parallel to the rough edges. The expressions for different types of scattering rates included in this study are discussed in the next section.

B. Instrinsic scattering rates and their expressions

The expression for the resistive umklapp scattering rate is taken from the work of Morelli *et al.* [32] and is given as $\tau_U^{-1}(\vec{q},b) = B_U\omega_{\vec{q},b}^{a_U}T^{b_U}e^{-\theta_b/3T}$, where $B_U = \frac{\hbar\gamma_b^2}{M\theta_b\bar{v}_b^2}$. $\bar{v}_b$ is the velocity of sound for each branch b and is calculated by the average slope of its dispersion curve near the Γ point [33],

γ_b is the Gruneisen parameter, θ_b is the Debye temperature of each phonon branch, and $\overline{M}$ is the average atomic mass of carbon. Here a_U and b_U are equal to 2 and 1, respectively, which have been used in innumerable studies conducted so far and produced excellent results.

An empirical form for normal scattering has been adopted from the paper by Morelli *et al.* [32]: $\tau_N^{-1}(\vec{q},b) = B_N \omega_{\vec{q},b}^{a_N} T^{b_N}$, where

$$B_N(a_N,b_N) = (k_B/\hbar)^{b_N} \frac{\hbar \gamma_b^2 v^{(a_N+b_N-2)/3}}{\overline{M} v^{a_N+b_N}}. \quad (7)$$

This simple model allows us to efficiently study a broad range of sizes and temperatures with good accuracy. Several studies have been carried out to determine the best empirical values for the constants a_N and b_N, which can accurately describe the contribution from momentum-conserving normal processes. For our study, we have used a_N and b_N to be 1 and 3, respectively, which has been used in several studies to explain the contribution from normal processes in materials such as diamond [34] and LiF [35] and fits experimental as well as first-principles data in quite good agreement. In particular, first-principles calculations predict a constant ($a_N = 0$) frequency dependence in pristine graphene; however, the constant dependence of the anharmonic scattering rate on phonon frequency was found to disappear in the presence of strain [36]. Even infinitesimally small amounts of strain were found to lead to a quadratic ($a_U = 2$) dependence for in-plane LA and TA branches and linear ($a_N = 1$) for the flexural ZA branch. This linear dependence can be also tied to the maximum scattering rate in the long-wavelength limit. In long-wavelength limit ($\omega \to 0$), the upper bound on the phonon scattering rate ($\Gamma_{\max} = 1/\tau_{\min}$) is dictated by the Ioffe-Regel limit [37]; equivalently, it can be obtained from Cahill's minimum thermal conductivity model [38], according to which $\omega\tau_{\min} = \pi$. In addition, as pointed out by Bonini *et al.* [36], for the quasiparticle criterion ($\omega\tau \geqslant 1$) to hold, the exponent a_N in $\tau_N^{-1}(\vec{q},b) \propto \omega_{\vec{q},b}^{a_N}$ has to be greater than or equal to 1 in the long-wavelength limit.

Naturally occurring isotopes of carbon can result in scattering due to the difference in their atomic masses. Thus, isotope scattering is also included while calculating the effective scattering rate and is given as [25] $\tau_{Iso}^{-1}(\omega) = (\Gamma\Omega_0/12)\omega^2 g(\omega)$, where the effective density of states is calculated by summing the density of states over all the branches b; $g(\omega) = \sum_b g_b(\omega)$. The mass-difference constant Γ is given by $\Gamma = \sum_i f_i(1 - M_i/\overline{M})^2 = c(1-c)/(12-c)^2$. The natural abundances of C^{12} and C^{13} are 98.9% and 1.1%, respectively, and thus, $c = 0.011$. The total intrinsic scattering rates can thus be mathematically expressed as

$$\frac{1}{\tau_{\text{int}}(\vec{q},b)} = \frac{1}{\tau_U(\vec{q},b)} + \frac{1}{\tau_N(\vec{q},b)} + \frac{1}{\tau_{Iso}(\omega)}. \quad (8)$$

C. Boundary scattering and contacts

In graphene nanoribbons, boundaries start playing a significant role in scattering of the heat carriers. As the edges of GNRs are not perfectly smooth, phonons tend to scatter from the boundaries and this effect becomes prominent with an increase in the rms value of edge roughness and decreased width of nanoribbons. In this work, the scattering rate due to line edge roughness (LER) is calculated in the same way as was done by Aksamija and Knezevic [39]. A momentum-dependent specularity parameter $p(\vec{q}) = \exp(-4q^2\Delta^2\sin^2\theta_E)$ has been introduced in order to accurately treat phonon scattering from edge roughness. It represents the ratio of specular reflections to the total number of interactions with the boundary. Δ represents the rms value of the line edge roughness and θ_E represents the angle made by incident phonons ($\vec{q}$) with the edge direction. The final expression for an effective LER scattering rate is given by [39]

$$\tau_{LER}^{-1}(\vec{q},b) = \frac{v_\perp(\vec{q},b)}{W} F_p(\vec{q}) \Big/ \left[1 - \frac{\Lambda_{\text{int}}^\perp(\vec{q},b)}{W} F_p(\vec{q})\right], \quad (9)$$

where $\Lambda_{\text{int}}^\perp(\vec{q},b) = v_\perp(\vec{q},b)\tau_{\text{int}}(\vec{q},b)$ is the phonon mean free path due to all the intrinsic processes (anharmonic phonon-phonon scattering and isotope scattering) across the ribbon perpendicular to edges. $v_\perp(\vec{q},b)$ is the velocity of phonons in the direction perpendicular to the rough edges and $\tau_{int.}(\vec{q},b)$ represents the relaxation time of phonons due to all intrinsic scattering processes. The complex interplay between line edge roughness scattering and internal scattering mechanisms for graphene ribbons is encapsulated in the parameter $F_p(\vec{q})$ called the form factor:

$$F_p(\vec{q}) = \frac{[1 - p(\vec{q})]\{1 - \exp[-W/\Lambda_{\text{int}}^\perp(\vec{q})]\}}{1 - p(\vec{q})\exp[-W/\Lambda_{\text{int}}^\perp(\vec{q})]}. \quad (10)$$

Contacts are assumed to be ideal and in equilibrium, which is captured by treating the interaction of phonons with the contacts analogously to the interaction of phonons with completely diffuse edges [$p(\vec{q}) = 0$] except having width (W) replaced by length (L) and the component of the phonon group velocity being taken along, rather than across, the ribbon. Thus, a length-dependent scattering term is given as $\tau_{\text{end}}^{-1}(\vec{q},b) = v_\parallel(\vec{q},b)/L\{1 - \exp[L/\Lambda_{\text{int}}^\parallel(\vec{q})]\}$, where $v_\parallel(\vec{q},b)$ is the velocity of phonons along the ribbon parallel to the rough edges and $\Lambda_{\text{int}}^\parallel(\vec{q},b)[= v_\parallel(\vec{q},b)\tau_{\text{int}}(\vec{q},b)]$ represents the phonon mean free path due to all intrinsic scattering processes along the ribbon direction. The scattering rates (normal, umklapp, isotope, and edge roughness) are added to get a total combined rate in suspended graphene as

$$\frac{1}{\tau_C(\vec{q},b)} = \frac{1}{\tau_{\text{int}}(\vec{q},b)} + \frac{1}{\tau_{LER}(\vec{q},b)} + \frac{1}{\tau_{\text{end}}(\vec{q},b)} \quad (11)$$

and thus can be used to calculate the resistive Debye term K_C and the nonresistive normal contribution K_N of thermal conductivity in GNRs.

III. RESULTS AND DISCUSSION

To study length dependence of thermal conductivity at room temperature, we scaled ribbon length while keeping the width constant ($W = 1.5$ μm) in order to mimic the experimental setup by Xu *et al.* [12]. In Fig. 1(a), thermal conductivity of freestanding graphene has been plotted against length for various discretization densities of the phonon dispersions. The red curve in Fig. 1(a) shows a convergence in thermal

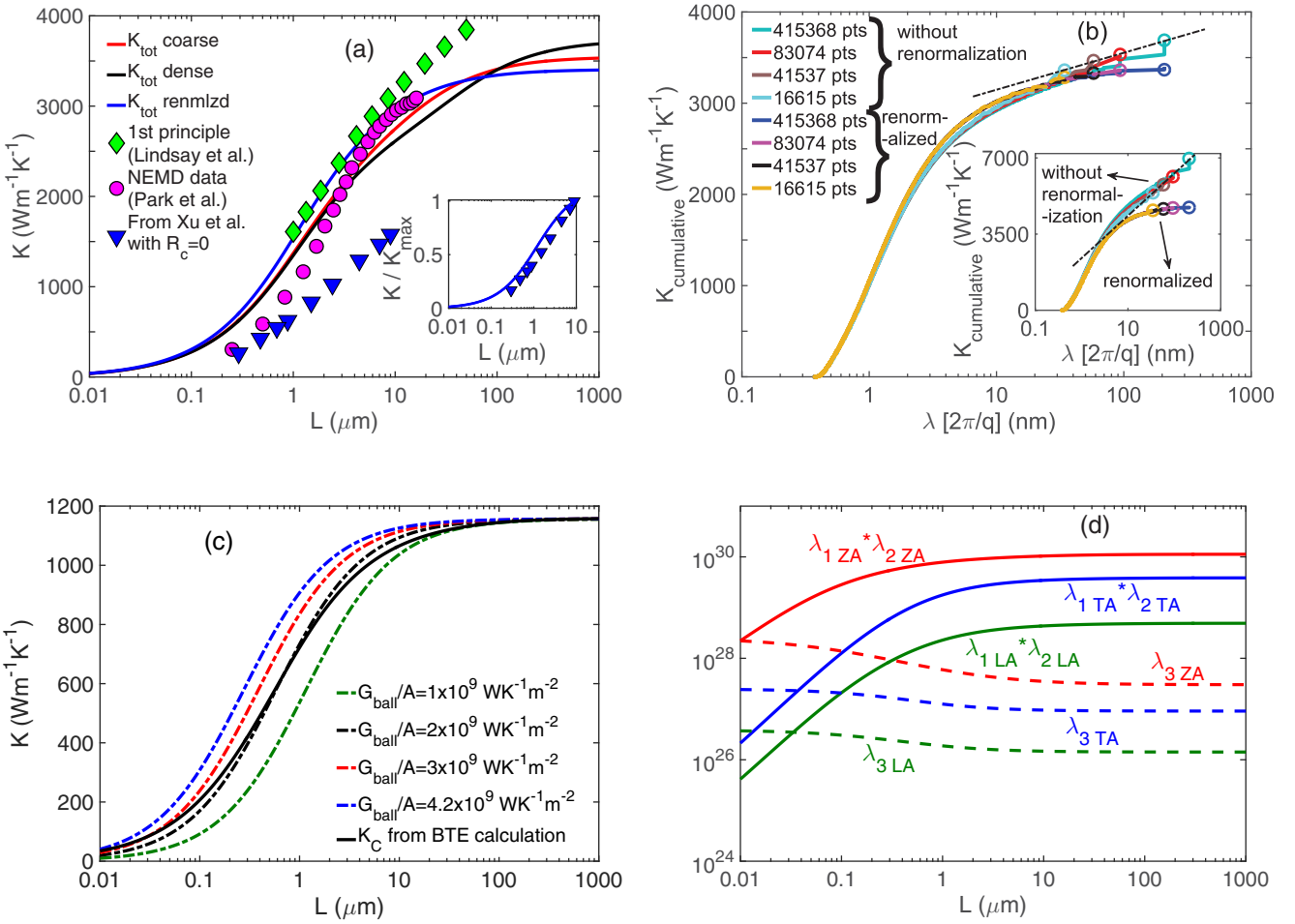

FIG. 1. (a) Convergence of thermal conductivity ($K_{\text{tot}} = K_C + K_N$) with length ($L$). Red and black solid lines (coincide for the most part) represent K_{tot} for coarse (83 074 points) and denser (415 368 points) discretization grids, respectively, with quadratic ZA modes, while the blue solid line in both (a) and (b) shows the convergence of thermal conductivity for the denser discretization grid with renormalized ZA dispersion. Diamond (in cyan) and circular (in magenta) markers represent first-principles data from Lindsay *et al.* [15] and NEMD simulation data from Park *et al.* [16], respectively. Inset: Comparison of our normalized thermal conductivity (blue solid line) with the normalized experimental data (blue triangles) for zero contact resistance from Xu *et al.* [12]. (b) Cumulative K_{tot} vs phonon wavelength for different grid densities for a finite graphene ribbon ($L = 1000$ μm, $W = 1.5$ μm, LER $= 2$ nm). Inset: Cumulative K_{tot} vs phonon wavelength for different grid densities for infinite graphene ($L = W = 1000$ μm, LER $= 0$ nm). (c) Compares resistive thermal conductivity (K_C represented by the black solid line) from our BTE calculations with $K_C(L)$ (resistive thermal conductivity as a function of L represented by dash-dotted lines) calculated from simple "gray" approximation [40] by fitting different $G_{\text{ballistic}}/A$ values. (d) Branchwise contribution of the correction factors in K_N ($\sum_b \frac{\lambda_1\lambda_2}{\lambda_3}$). For (a)–(d) the width and rms value of edge roughness (LER) used are 1.5 μm and 2 nm, respectively, and temperature is 300 K.

conductivity for a coarse discretization of q points having 83 074 points in the first Brillouin zone. Previous studies suggest that a major part of thermal conductivity comes from the quadratic out-of-plane ZA modes and divergence is a consequence of the long-wavelength problem. Klemens [41] was among the first to propose a logarithmic divergence of thermal conductivity in the two-dimensional phonon gas. In his simplified umklapp-limited model, the spectral specific heat [$C(\omega)$] in two dimensions is proportional to ω, while the intrinsic mean free path $l_i(\omega) \propto \omega^{-2}$ T assumes a quadratic umklapp scattering rate and linear dispersion. Klemens then attributed the logarithmic divergence to the problem of long waves: in the limit $q \to 0$, as the phonon wavelength gets larger, the spectral phonon density [$N(\omega) = n_0(\omega)g(\omega) \propto 1/\omega$] diverges, leading to a logarithmic divergence in the resulting thermal conductivity integral [31].

A. Numerical convergence and renormalization of ZA modes

In order to treat the problem of long waves more accurately, we repeated our calculation of thermal conductivity keeping all parameters exactly the same, but employing a much denser discretization grid of q points having 415 368 points for the dispersion and numerical integration. We obtained a similar converging behavior but with larger values of thermal conductivity at $L = 1000$ μm, as shown by the black curve in Fig. 1(a), than the one obtained from a coarser grid of 83 074 points (shown by the red curve in the same figure). This led us to further investigate convergence in the long-wavelength limit and consequently, we plotted cumulative thermal conductivity as a function of phonon wavelength for different densities of grid discretization as shown in Fig. 1(b). In Fig. 1(b), for all discretization densities (without renormalization), steps can be observed at the largest wavelength in the discretization,

indicating an increase in thermal conductivity due to the addition of more long-wavelength phonons. Despite adding more discretization of q points around $q \to 0$ by making the dispersion grid denser, the results still do not converge fully as shown by the dashed black line joining the total cumulative thermal conductivity for different grid densities. This behavior is even more prominent in the case of infinite graphene ($L = W = 1000$ μm, LER = 0 nm) as shown by the dashed black line in the inset of Fig. 1(b). So we conclude that the convergence observed in Fig. 1(a) is not an actual convergence but rather a numerical one, caused by the finite number of discretization points. Thus our results show that even for a ribbon with fixed width and diffuse edges, thermal conductivity diverges with length as long as the dispersion of the out-of-plane ZA modes is quadratic.

However, there are many studies in the literature showing how strain due to various effects [e.g., temperature expansion (crumpling), in-plane-to-cross-plane coupling, and several others] affects the flexural modes in the long-wavelength regime. Castro Neto *et al.* [42] and Xu *et al.* [43] show the effect of thermal stress on flexural modes in freestanding graphene, and long-wavelength ZA modes are reported to be completely linearized ($\omega \propto q$). Several recent studies [44] have shown that increasing the size of the free-standing graphene will gradually cause a stiffening of the flexural modes, arising out of the coupling between in-plane and out-of-plane modes. This coupling has also been found to result in renormalization of ZA modes; however, flexural phonon modes are reported to be partially linearized ($\omega \propto q^{1.5}$). The blue curve in Figs. 1(a) and 1(b) represents thermal conductivity with dense discretization grid and partially linearized (renormalized) ZA dispersion, i.e., with $\omega \propto q^{1.5}$ (renormalization will be further discussed in the next section). This stiffening of ZA modes causes convergence of thermal conductivity with length and leads to a finite value of thermal conductivity, as evidenced by the smooth convergence and the lack of large steps in the long-wavelength limit [Fig. 1(b), for both finite and infinite graphene]. Good agreement between our result (solid blue line) and previously reported first-principles [15] [cyan-colored diamond markers in Fig. 1(a)] and molecular dynamics [16] calculations [magenta-colored circular markers in Fig. 1(a)] confirm that the improved Callaway model can be used as an effective tool for the treatment of momentum-conserving normal processes. Our calculated thermal conductivity, when scaled with $K_{\max}$ to compensate for contact resistance in the experiments, follows the same trend as that of the measured data [12], shown in the inset of Fig. 1(a).

B. Analytical calculations

Here, the analysis of the divergence of thermal conductivity with length is generalized to include the quadratic dispersion of the ZA branch and the nonresistive normal contribution, both of which were ignored in previous analyses. For a general dispersion of the form $\omega \propto q^s$, frequency dependence of the group velocity [$\vec{v}(\vec{q}) = \nabla\omega(\vec{q})$] is given as $v \propto \omega^{(s-1)/s}$, while the density of states $D(\omega) \propto \omega^{(2-s)/s}$. In the long-wavelength limit ($\omega \to 0$) and for finite width, the resistive part of thermal conductivity (K_C) is mainly dominated by edge roughness scattering which, according to Eq. (9), varies as $\tau_{LER}^{-1}(\omega) \propto v(\omega)$. Thus the resistive part of thermal conductivity [$K_C(\omega)$] $\propto v^2(\omega)\tau_{LER}D(\omega) \propto \omega^{(1/s)}$ indicating that K_C converges with length and reaches the diffusive regime as long as we maintain finite width of the samples, irrespective of the value of the exponent s, as our results in Fig. 1(c) indicate.

The length dependence of the resistive component of thermal conductivity (K_C) can be captured through a simple Landauer model [45,46], where the heat conduction is described by constant thermal conductance (G) in the ballistic regime. Then the length variation in K_C is well described by a transition from the ballistic to the diffusive regime as $K(L) = [A/(LG_{\text{ball}}) + 1/K_{\text{diff}}]^{-1}$ [40]. Setting $(G_{\text{ball}}/A) = 2 \times 10^9$ W K^{-1} m^{-2} exactly fits the resistive part of thermal conductivity as shown in Fig. 1(c). The mean free path (λ) is calculated from this value by angle averaging in 2D as $K_{\text{diff}} = (G_{\text{ball}}/A)(\pi/2)\lambda$. The mfp of phonons in suspended graphene with rough boundaries and $W = 1.5$ μm is thus calculated to be 358 nm, somewhat smaller than previously reported values of around 800 nm for large square samples [47] due to the presence of edge roughness of 2 nm in our case. Hence we conclude that the resistive contribution to the thermal conductivity is undergoing a simple ballistic-to-diffusive transition as length is increased, saturating when $L > 10$ μm.

On the other hand, the length dependence of thermal conductivity of long ribbons ($L > 1$ μm) is dominated by the hydrodynamic contribution, represented by K_N, and its length dependence is different from what can be observed in ballistic regime. The nonresistive normal contribution (K_N) is comprised of three factors: λ_1, λ_2, and λ_3, where by analysis analogous to that for K_C, we find that $\lambda_2 \propto \omega^{(3-s)/s}$ and $\lambda_3 \propto \omega^{(5-2s)/s}$ [based on Eqs. (5) and (6)]. Thus for $s \leqslant 2.5$ both λ_2 and λ_3 will converge with increasing length. However, $\lambda_1 \propto \omega^{(3-2s)/s}$ and thus, for a purely quadratic dispersion ($s = 2$) λ_1 diverges and consequently, the total thermal conductivity (K_{tot}) will not converge even in the presence of edge roughness (λ_1 would converge only when $s \leqslant 1.5$). This is evident in Fig. 1(b) where red and black curves show a continuing step behavior as length is increased; we obtain a finite value only because our discretization is finite and length eventually exceeds the largest phonon wavelength captured in the long-wavelength limit.

As we noted earlier, Mariani and von Oppen [44] reported that increasing the size of the graphene sheet leads to stiffening of the flexural modes due to the coupling force between bending and stretching degrees of freedom, thereby causing renormalization of flexural modes as $\omega_{ZA} = \beta_{ZA}(q)q^2$ where $\beta_{ZA}(q) = \alpha_{ZA}[1 + (q_c/q)^2]^{1/4}$, q_c being the cut-off wave vector. The temperature-dependent transition point q_c is calculated to be 0.1 (in the units of 2π/lattice constant) [44]. When $L \to \infty$ ($q \to 0$), $q_c \gg q$ and ω_{ZA} becomes proportional to $q^{3/2}$. Renormalization of ZA modes and their partial linearization in the long-wavelength regime (where $s = 3/2$) causes λ_1 ($\propto \omega^{(3-2s)/s}$), λ_2 ($\propto \omega^{(3-s)/s}$), and λ_3 ($\propto \omega^{(5-2s)/s}$) all to converge with length, as can be seen in Fig. 1(d). Therefore the nonresistive normal contribution (K_N) eventually converges to a finite value owing to the coupling between the in-plane and out-of-plane degrees of freedom. The solid blue curve in Figs. 1(a) and1(b) show convergence of thermal conductivity with length to a bulk value of 3400 W m^{-1} K^{-1} for ribbon

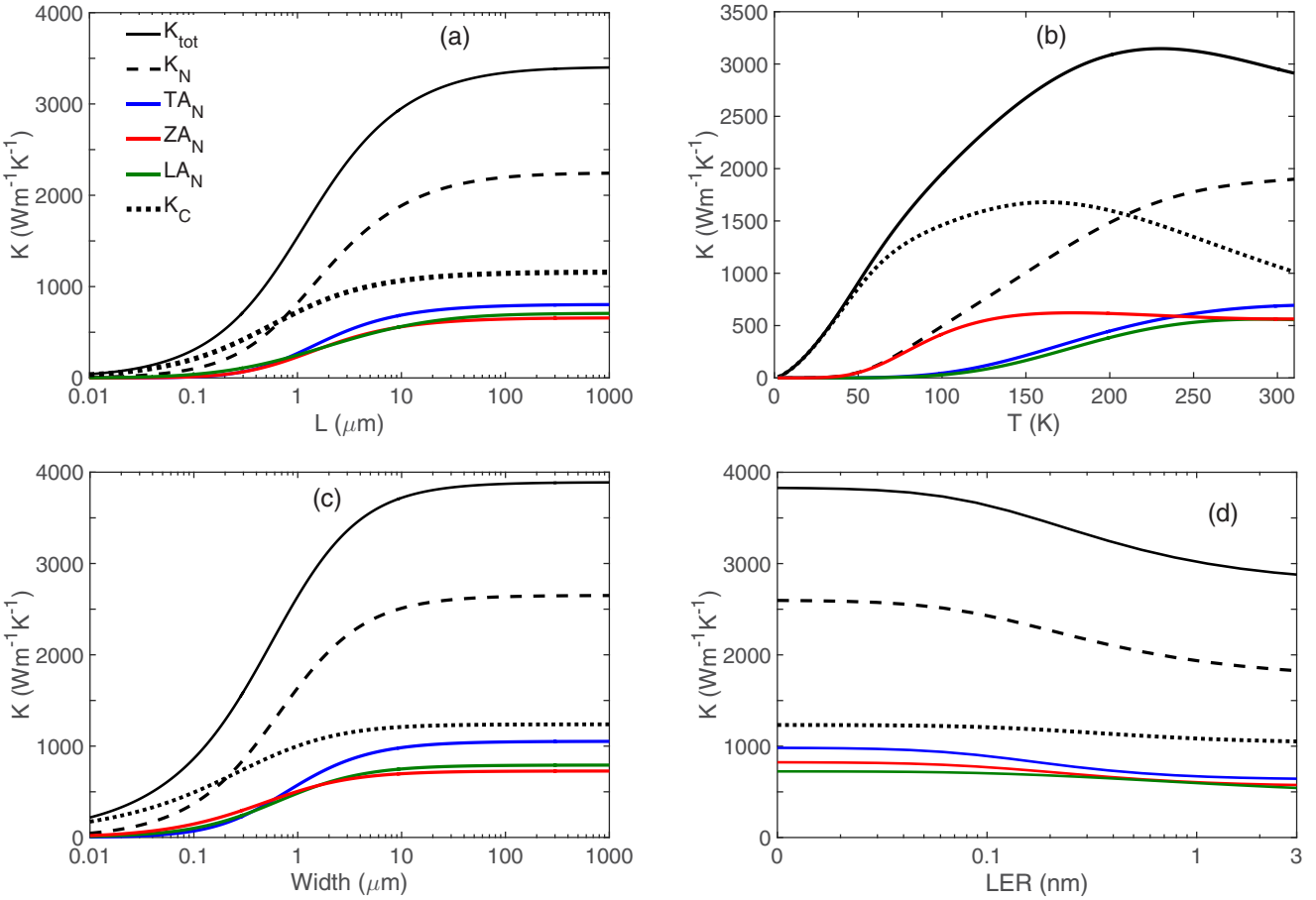

FIG. 2. (a) Branchwise contribution of thermal conductivity against length (L) of GNRs. Black solid and dashed lines [in (a)–(d)] represent total thermal conductivity ($K_{\rm tot} = K_C + K_N$) and nonresistive normal contribution (K_N), respectively, and black dotted lines [(in (a)–(d)] represent resistive contribution (K_C). Blue, green, and red curves [(in (a)–(d)] represent TA, LA, and ZA components of K_N, respectively. (b) Effect of temperature on the contribution of $K_{\rm tot}$, K_C, and K_N. (c) shows the width dependence of $K_{\rm tot}$, K_C, and K_N. (d) represents the effect of edge roughness on $K_{\rm tot}$, K_C, and K_N. Length of GNRs [in (b)–(d)] is 10 μm. Width [in (a), (b), and (d)] is 1.5 μm and temperature [in (a), (c), and (d)] is 300 K.

width of 1.5 μm, in good agreement with both experimental measurements and first-principles calculations [48]. We have also computed cumulative thermal conductivity against phonon wavelength for different values of q_c (0.01, 0.05, and 0.2 in the units of 2π/lattice constant) and found that the convergence in the long-wavelength limit as shown in Fig. 1(b) is independent of q_c.

However, it should be noted that besides the strain induced due to coupling between the in-plane and out-of-plane modes as studied by Mariani and von Oppen [44], there are other studies in the literature reporting different kinds of renormalization. Castro Neto *et al.* [42] and Xu *et al.* [43] gave an expression of the form $\omega_{ZA} = q\sqrt{\frac{\kappa q^2+S}{\rho}}$, where κ is the bending rigidity of graphene, ρ is the mass density, and S is the surface tension. This expression can be rearranged to a form $\omega_{ZA} = q^2\alpha_{ZA}[1+(q_c/q)^2]^{1/2}$, where $\alpha_{ZA} = \sqrt{\kappa/\rho}$, and $q_c = \sqrt{S/\kappa}$. In both of these cases [42,43], the dispersion of flexural modes becomes linearized ($\omega_{ZA} \propto q$) in the long-wavelength limit ($q \to 0$) under tension. We show in our analytical calculations that for any dispersion of the general form $\omega \propto q^s$, all the terms K_C, λ_1, λ_2, and λ_3 converge as long as $s \leqslant 1.5$. Thus we conclude that, irrespective of whether the dispersion of ZA modes gets partially linearized ($\omega_{ZA} \propto q^{1.5}$) or completely linearized ($\omega_{ZA} \propto q$) due to tension, $K_{\rm tot}$ converges to a finite value.

Figure 2(a) shows branchwise components of thermal conductivity and their length dependence. Earlier studies have shown that length divergence in thermal conductivity is due to quadratic dispersion of out-of-plane modes; however, because of the coupling between the in-plane and flexural modes renormalization of ZA dispersion takes place, which leads to partial linearization of flexural modes and thereby causes thermal conductivity to converge when $L \to \infty$ in the long-wavelength limit. We observe here that the divergence in K_N beyond 10 μm is driven by the out-of-plane ZA branch, but renormalization of the ZA branch prevents λ_1 [Eq. (4)] from diverging (for $s = 3/2$, $\lambda_1 \propto \omega^{(3-2s)/s} = \text{const}$) and the hydrodynamic component eventually reaches saturation for $L > 100$ μm, indicating the onset of the Ziman regime where extrinsic effects such as length no longer play a role.

C. Temperature, width, and LER dependence

We used a sample of 10 μm long and 1.5 μm wide to study the effect of temperature and LER on thermal

conductivity in graphene ribbons. In Fig. 2(b), thermal conductivity (K_{tot}) along with its resistive (K_C) and nonresistive normal components (K_N) are plotted against temperature. At low temperatures, thermal conductivity is mainly comprised of resistive contribution, while at room temperature and above, the resistive contribution is suppressed considerably due to strong umklapp phonon-phonon scattering and nonresistive normal contribution starts playing an important role. Thus in graphene, K_C fails to capture the contribution coming from momentum-conserving normal processes and leads to underevaluation of thermal conductivity at and above room temperatures. It can also be seen that at low temperatures, the out-of plane (ZA) modes coming from K_C contribute significantly to thermal conductivity, whereas at high temperatures, most of the conductivity comes from the hydrodynamic contribution (represented by K_N) of the in-plane branches (LA and TA).

Next we turn to the width dependence of thermal conductivity in suspended graphene ribbons at room temperature and vary the width W while keeping $L = 10$ μm and a constant edge roughness $\Delta = 2$ nm, which puts the ribbons in the fully diffusive edge scattering regime. It can be seen in Fig. 2(c) that the resistive part of thermal conductivity (K_C) shows a gradual width dependence. It is because for ribbons narrower than 200 nm, the ribbon is in the ballistic regime where both K_C is suppressed by LER scattering ($\tau_{LER}^{-1} \propto 1/\mathrm{W}$). In this range, the contribution from nonresistive processes (K_N) is also significantly reduced by the presence of resistive LER scattering, whereas widths above 200 nm put the ribbon in the Poiseuille regime [49]. In the Poiseuille flow range, where 200 nm $\leqslant W \leqslant 10$ μm, the K_N is affected by the interplay of LER scattering and normal scattering, leading to a pronounced width dependence exceeding that of the resistive component. The contribution of the nonresistive normal processes to width dependence has not been previously reported and can be understood as a consequence of the hydrodynamic phonon transport suggested by Lee *et al.* [49]. Beyond 10 μm, K_N transitions into the Casimir regime where normal processes dominate over resistive LER scattering and the thermal conductivity again converges to a finite value.

Unlike their supported counterparts, LER scattering plays a very crucial role in the thermal conductivity of suspended graphene ribbons. Figure 2(d) shows a strong dependence of thermal conductivity (K_{tot}) for edge roughness up to 0.5 nm (rms value). In this figure, it can be seen that K_{tot} corresponding to zero edge roughness is the same as that of K_{tot} for a 1000-μm-wide ribbon as can be seen in Fig. 2(c), which again indicates that for such wide ribbons the effect of edge roughness completely dies off. The effect of the edge roughness and width of the ribbons cannot be completely decoupled. As we keep on reducing, the width of the ribbon from 1000 μm with fixed edge roughness is equivalent to increasing the edge roughness for a given width of the ribbon. K_N shows a strong LER dependence up to 0.5 nm, whereas K_C shows weaker dependence on edge roughness as is the case for width dependence of thermal conductivity.

IV. CONCLUSION

In conclusion, we have studied the length divergence of suspended graphene ribbons, employing the newly developed improved Callaway model to accurately capture the significant contribution from the nonresistive normal processes in the hydrodynamic regime. We have shown through both numerical and analytical calculations that this nonresistive normal contribution dominates the length dependence for lengths greater than 1 μm and leads to a logarithmic divergence, even in ribbons with fixed width and edge roughness. This divergence is caused by the combination of the quadratic dispersion of the out-of-plane ZA phonon branch in the long-wavelength limit.

However, for lengths exceeding 100 μm, we find that thermal conductivity converges to a constant value. This convergence is independent of width and not caused by edge disorder; rather, it is due to linearization of the ZA branch by coupling between the in-plane and out-of-plane degrees of freedom. This coupling removes the quadratic dependence of the ZA dispersion and limits the normal contribution of the ZA branch to a finite value. We also uncover a prominent width dependence arising from the nonresistive normal contribution for widths exceeding 200 nm, which delineates the emergence of Pouiselle hydrodynamic heat flow. Our study confirms the role of nonresistive normal processes in the length and width scaling of thermal conductivity and provides quantitative limits to the hydrodynamic regime of heat flow in graphene ribbons.

ACKNOWLEDGMENT

This work was supported by the National Science Foundation through Award 1542864.

[1] Alexander A. Balandin, Suchismita Ghosh, Wenzhong Bao, Irene Calizo, Desalegne Teweldebrhan, Feng Miao, and Chun Ning Lau, Superior thermal conductivity of single-layer graphene, Nano Lett. **8**, 902 (2008).

[2] Jae-Ung Lee, Duhee Yoon, Hakesong Kim, and Sang Wook Lee, and Hyeonsik Cheong, Thermal conductivity of suspended pristine graphene measured by Raman spectroscopy, Phys. Rev. B **83**, 081419 (2011).

[3] S. Chen, Arden L. Moore, Weiwei Cai, Ji Won Suk, Jinho An, Columbia Mishra, Charles Amos, Carl W. Magnuson, Junyong Kang, Li Shi, and Rodney S. Ruoff, Raman measurements of thermal transport in suspended monolayer graphene of variable sizes in vacuum and gaseous environments, ACS Nano **5**, 321 (2011).

[4] Jian-Hao Chen, Chaun Jang, Shudong Xiao, Masa Ishigami, and Michael S. Fuhrer, Intrinsic and extrinsic performance limits of graphene devices on SiO_2, Nat. Nanotechnol. **3**, 206 (2008).

[5] Alexander A. Balandin, Thermal properties of graphene and nanostructured carbon materials, Nat. Mater. **10**, 569 (2011).

[6] Jae Hun Seol, Insun Jo, Arden L. Moore, Lucas Lindsay, Zachary H. Aitken, Michael T. Pettes, Xuesong Li, Zhen Yao, Rui Huang, David Broido, Natalio Mingo, Rodney S. Ruoff, and Li Shi, Two-dimensional phonon transport in supported graphene, Science **328**, 213 (2010).

[7] Baowen Li and Jiao Wang, Anomalous Heat Conduction and Anomalous Diffusion in One-Dimensional Systems, Phys. Rev. Lett. **91**, 044301 (2003).

[8] Abhishek Dhar, Heat transport in low-dimensional systems, Adv. Phys. **57**, 457 (2008).

[9] Onuttom Narayan and Sriram Ramaswamy, Anomalous Heat Conduction in One-Dimensional Momentum-Conserving Systems, Phys. Rev. Lett. **89**, 200601 (2002).

[10] Tomaž Prosen and David K. Campbell, Momentum Conservation Implies Anomalous Energy Transport in 1D Classical Lattices, Phys. Rev. Lett. **84**, 2857 (2000).

[11] C. W. Chang, D. Okawa, H. Garcia, A. Majumdar, and A. Zettl, Breakdown of Fourier's Law in Nanotube Thermal Conductors, Phys. Rev. Lett. **101**, 075903 (2008).

[12] Xiangfan Xu, Luiz F. C. Pereira, Yu Wang, Jing Wu, Kaiwen Zhang, Xiangming Zhao, Sukang Bae, Cong Tinh Bui, Rongguo Xie, John T. L. Thong, Byung Hee Hong, Kian Ping Lo, Davide Donadio, Baowen Li, and Barbaros Özyilmaz, Length-dependent thermal conductivity in suspended single-layer graphene, Nat. Commun. **5**, 3689 (2014).

[13] S. Mei, L. N. Maurer, Z. Aksamija, and I. Knezevic, Full-dispersion Monte Carlo simulation of phonon transport in micron-sized graphene nanoribbons, J. Appl. Phys. **116**, 164307 (2014).

[14] D. L. Nika, S. Ghosh, E. P. Pokatilov, and A. A. Balandin, Lattice thermal conductivity of graphene flakes: Comparison with bulk graphite, Appl. Phys. Lett. **94**, 203103 (2009).

[15] L. Lindsay, Wu Li, Jesús Carrete, Natalio Mingo, D. A. Broido, and T. L. Reinecke, Phonon thermal transport in strained and unstrained graphene from first principles, Phys. Rev. B **89**, 155426 (2014).

[16] Park Minkyu, Sun-Chul Lee, and Yong-Sung Kim, Length-dependent lattice thermal conductivity of graphene and its macroscopic limit, J. Appl. Phys. **114**, 053506 (2013).

[17] Giuliana Barbarino, Claudio Melis, and Luciano Colombo, Intrinsic thermal conductivity in monolayer graphene is ultimately upper limited: A direct estimation by atomistic simulations, Phys. Rev. B **91**, 035416 (2015).

[18] Philip B. Allen, Improved Callaway model for lattice thermal conductivity, Phys. Rev. B **88**, 144302 (2013).

[19] Qiu Bo and Xiulin Ruan, Reduction of spectral phonon relaxation times from suspended to supported graphene, Appl. Phys. Lett. **100**, 193101 (2012).

[20] Kin Chung Fong and K. C. Schwab, Ultrasensitive and Wide-Bandwidth Thermal Measurements of Graphene at Low Temperatures, Phys. Rev. X **2**, 031006 (2012).

[21] Nuo Yang, Xiaoxi Ni, Jin-Wu Jiang, and Baowen Li, How does folding modulate thermal conductivity of graphene?, Appl. Phys. Lett. **100**, 093107 (2012).

[22] Zhen Huang, Timothy S. Fisher, and Jayathi Y. Murthy, Simulation of phonon transmission through graphene and graphene nanoribbons with a Green's function method, J. Appl. Phys. **108**, 094319 (2010).

[23] P. G. Klemens, and D. F. Pedraza, Thermal conductivity of graphite in the basal plane, Carbon **32**, 735 (1994).

[24] D. L. Nika, E. P. Pokatilov, A. S. Askerov, and A. A. Balandin, Phonon thermal conduction in graphene: Role of umklapp and edge roughness scattering, Phys. Rev. B **79**, 155413 (2009).

[25] Z. Aksamija and I. Knezevic, Lattice thermal conductivity of graphene nanoribbons: Anisotropy and edge roughness scattering, Appl. Phys. Lett. **98**, 141919 (2011).

[26] Zhiyong Wei, Juekuan Yang, Kedong Bi, and Yunfei Chen, Mode dependent lattice thermal conductivity of single layer graphene, J. Appl. Phys. **116**, 153503 (2014).

[27] Enrique Muñoz, Jianxin Lu, and Boris I. Yakobson, Ballistic thermal conductance of graphene ribbons, Nano Lett. **10**, 1652 (2010).

[28] Andrea Cepellotti, Giorgia Fugallo, Lorenzo Paulatto, Michele Lazzeri, Francesco Mauri, and Nicola Marzari, Phonon hydrodynamics in two-dimensional materials, Nat. Commun. **6**, 6400 (2015).

[29] Joseph Callaway, Model for lattice thermal conductivity at low temperatures, Phys. Rev. **113**, 1046 (1959).

[30] Jinlong Ma, Wu Li, and Xiaobing Luo, Examining the Callaway model for lattice thermal conductivity, Phys. Rev. B **90**, 035203 (2014).

[31] L. Lindsay, D. A. Broido, and Natalio Mingo, Flexural phonons and thermal transport in graphene, Phys. Rev. B **82**, 115427 (2010).

[32] D. T. Morelli, J. P. Heremans, and G. A. Slack, Estimation of the isotope effect on the lattice thermal conductivity of group IV and group III-V semiconductors, Phys. Rev. B **66**, 195304 (2002).

[33] B. D. Kong, S. Paul Nardelli, M. Buongiorno, and K. W. Kim, First-principles analysis of lattice thermal conductivity in monolayer and bilayer graphene, Phys. Rev. B **80**, 033406 (2009).

[34] N. V. Novikov, A. P. Podoba, S. V. Shmegera, A. Witek, A. M. Zaitsev, A. B. Denisenko, W. R. Fahrner, and M. Werner, Influence of isotopic content on diamond thermal conductivity, Diam. Relat. Mater. **8**, 1602 (1999).

[35] R. Berman and J. C. F. Brock, The effect of isotopes on lattice heat conduction. I. Lithium fluoride, Proc. R. Soc. London, Ser. A **289**, 46 (1965).

[36] Nicola Bonini, Jivtesh Garg, and Nicola Marzari, Acoustic phonon lifetimes and thermal transport in free-standing and strained graphene, Nano Lett. **12**, 2673 (2012).

[37] M. Gurvitch, Ioffe-Regel criterion and resistivity of metals, Phys. Rev. B **24**, 7404 (1981).

[38] David G. Cahill, S. K. Watson, and R. O. Pohl, Lower limit to the thermal conductivity of disordered crystals, Phys. Rev. B **46**, 6131 (1992).

[39] Z. Aksamija and I. Knezevic, Thermal transport in graphene nanoribbons supported on SiO_2, Phys. Rev. B **86**, 165426 (2012).

[40] Myung-Ho Bae, Zuanyi Li, Zlatan Aksamija, Pierre N. Martin, Feng Xiong, Zhun-Yong Ong, Irena Knezevic, and Eric Pop, Ballistic to diffusive crossover of heat flow in graphene ribbons, Nat. Commun. **4**, 1734 (2013).

[41] P. G. Klemens, Theory of thermal conduction in thin ceramic films, Int. J. Thermophys. **22**, 265 (2001).

[42] A. H. Castro Neto, F. Guinea, N. M. R. Peres, K. S. Novoselov, and A. K. Geim, The electronic properties of graphene, Rev. Mod. Phys. **81**, 109 (2009).

[43] P. Xu, M. Neek-Amal, S. D. Barber, J. K. Schoelz, M. L. Ackerman, P. M. Thibado, A. Sadeghi, and F. M. Peeters, Unusual ultra-low-frequency fluctuations in freestanding graphene, Nat. Commun. **5**, 3720 (2014).

[44] Eros Mariani and Felix von Oppen, Flexural Phonons in Free-Standing Graphene, Phys. Rev. Lett. **100**, 076801 (2008).

[45] Prasher Ravi, Thermal boundary resistance and thermal conductivity of multiwalled carbon nanotubes, Phys. Rev. B **77**, 075424 (2008).

[46] Changwook Jeong, Supriyo Datta, and Mark Lundstrom, Full dispersion versus Debye model evaluation of lattice thermal conductivity with a Landauer approach, J. Appl. Phys. **109**, 073718 (2011).

[47] S. Ghosh, I. Calizo, D. Teweldebrhan, E. P. Pokatilov, D. L. Nika, A. A. Balandin, W. Bao, F. Miao, and C. N. Lau, Extremely high thermal conductivity of graphene: Prospects for thermal management applications in nanoelectronic circuits, Appl. Phys. Lett. **92**, 151911 (2008).

[48] G. Fugallo, A. Cepellotti, L. Paulatto, M. Lazzeri, N. Marzari, and F. Mauri, Thermal conductivity of graphene and graphite: Collective excitations and mean free paths, Nano Lett. **14**, 6109 (2014).

[49] Sangyeop Lee, David Broido, Keivan Esfarjani, and Gang Chen, Hydrodynamic phonon transport in suspended graphene, Nat. Commun. **6**, 6290 (2015).